This project has received funding from the European Union's Horizon 2020 research and innovation programme under grant agreement No 871813.

MUNDFAB

ICT Project No 871813

MUNDFAB

Modeling Unconventional Nanoscaled Device FABrication

D4.1: Specification report for LA calibration: literature review, missing data, experimental plan

A. La Magna(CNR), P. Pichler (Fraunhofer), F. Cristiano (LAAS-CNRS), I. Deretzis (CNR), B. Sklenard (CEA), I. Bejenari (Fraunhofer), P. Michalowski (ITME), D. Rideau (STM), T. Grasser (TUW)

July 03, 2020

Fraunhofer IISB leti ceatech cnrs Łukasiewicz Instytut Technologii Materiałów Elektronicznych life.augmented TU WIEN

Quality management

This deliverable was reviewed by:

Anne Hemeryck (LAAS-CNRS)

Eberhard Baer (Fraunhofer)

Contents

Executive Summary

This document reports, in a specification format, the first version of the calibration integrated in the Laser Annealing simulation tools. The calibration is derived by means of a literature analysis and it focuses on a list of materials of interest. This list has been determined in dedicated meetings among the partners and it considers materials which should potentially be part of the device structure before the laser process. The information reported in the MUNDFAB Deliverable 6.1 “Device architectures and processing of the test applications” has been specifically considered for the compilation of this list.

The calibration is presented in a sequence of tables which specify values or functional dependences of the variables for key parameters, including reference sources. A brief discussion commenting the data is also reported. Laser annealing simulations, which will be performed by means of the customized tools at the CNR and CEA in the early stage of the project, will use this calibration. Calibration improvements will be pursued during the project and any advancement will be properly disseminated.

The report additionally discusses the experimental plan which will be implemented to improve the calibration with focused direct optical measurements. Moreover, we will also present the experimental studies of the process in blanket and 2D/3D constrained geometries.

Due to the interrelationship of this topic, at least one representative of each partner has been involved in its preparation whereas the CNR is the main owner of D4.1.

1. Introduction

Laser annealing (LA) with pulsed power emission (pulse duration below 10^{-6} s) allows for focalized heating in confined submicrometric regions. As a consequence, it is the application of choice in complex integration schemes where a thermal budget is necessary in very small regions whilst other zones of the irradiated structure must be shielded by the heating. Of course, due to the specificity of the electromagnetic energy absorption and the ultra-rapid thermal diffusion, the potential benefits of LA are somehow weakened by a penalty in terms of a complex process design, which maybe is unique in microelectronics and overlaps with the device design (i.e. its geometry and the used materials). Considering this complexity of the Design of Experiments (DoE) for the optimization of the LA process, the corresponding process simulations are essential tools to drastically reduce the real DoE with the aid of a virtual DoE. The MUNDFAB project, dealing with the advanced TCAD of processes characterized by a low thermal budget, has dedicated WP4 to the simulation of LA processes. Among the various themes considered in WP4, a critical one is the calibration of the materials' parameters, which should be assessed as soon as possible in order to allow the full predictivity of the models.

In this report we will discuss the current status of the model calibration for a list of materials of interest in the project. The decision on the material list has been achieved by means of a series of meetings among the partners. In spite of the particular realization of real LA processes and their integration in the manufacturing flow, which are beyond the scopes of MUNDFAB, this list considers the materials which should potentially compose the devices structures (see also D6.1) before the laser processes. As a fallout of the analysis on the current calibration reliability and on the missing data we will also present the plan of the future experimental activity in WP4.

2. Reference materials and preliminary parameters calibration

Simulations of Laser Annealing processes require an accurate calibration of the optical and thermal properties of key device materials (including metals, nitrides and oxides) over the entire temperature range of the LA process (e.g. from RT to 2000K and more) and for all involved phases (crystal, amorphous and liquid) in the case of materials which can manifest phase transition during the process (namely the semiconductor materials). Table 1 lists the materials that will be considered for the fabrication of device test structures, where LA processes will be performed. The experimental characterization on these systems will allow for the validation of the simulation results by means of comparisons. Indeed, as we will discuss in detail in section 4, dopant profiles, alloy fraction redistributions and the overall structural modifications can be predicted and compared with the corresponding experimental characterizations.

The required phases and relevant critical issues (in terms of missing data) are indicated by symbols and color codes.

Material	crystal	amorphous	liquid	alloy fraction
Silicon	✓	✓	✓	✗
Germanium	✓	✓	✓	✗
SiGe	✓	✓	✓	✓
SiO_2	✗	✓	✗	✗
HfO_2	✗	✓	✗	✗
Si_3N_4	✗	✓	✗	✗
SiN	✗	✓	✗	✗
TiN	✓	✗	✗	✗
W	✓	✗	✗	✗
Pt	✓	✗	✗	✗

Tab. 1: Materials list. Checkmarks indicate the material phases that have to be considered in the calibration while the crosses indicate phases which are not considered in the processing/simulations. The green color indicates sufficiently reliable data, the orange indicates a mandatory calibration improvement, while red indicates insufficient or missing data.

Irradiation experiments will be performed with the equipment installed in the CEA-LETI laboratories. The laser source has a wave length of λ=308 nm and as a consequence the optical parameters will be calibrated considering this specific wave length. A generalization of the approach to a different laser source would require a revision of the optical parameters only. Nanosized effects on the thermal transport coefficient will not be discussed here: they are specific investigations of Task 4.3. In the following subsections we will report the calibration parameters for the materials listed in the table 1. This calibration will be integrated in the customized codes at CNR and CEA for the preliminary simulations within the MUNDAFAB project and it will be subject of refinement as a consequence of the overall activity in the WP4. We notice that in some formulas we use the notations like ($T \geq T^*$) or ($T < T^*$) to indicate the Heaviside step functions (e.g. ($T < T^*$) means 1 for $T<T^*$ and 0 for $T \geq T^*$), see for instance line 6 in table 2. If expressions are multiplied by a step function, the continuity constrain is always imposed in the whole range of the variable. Analytic formulas are parsed by the laser annealing code material database. As a consequence, if only rough data or figures are reported in the cited references, the reported expressions correspond to a reliable fitting of these data.

Silicon

The material database needed for laser annealing of Silicon substrates is reliable for the solid and the liquid phase due to the large number of investigations dealing with the LA process of Silicon (see table 1). For this material all three phases (i.e. c-Si, l-Si and $\boldsymbol{\alpha}$-Si) have to be considered. Amorphous phase parameters in the literature have a natural spread due to the possible dependence of physical parameters on the $\boldsymbol{\alpha}$-phase preparation (e.g. implantation, deposition etc). Anyhow, a preliminary parameter set will be presented as a basis of the joint simulation and experimental work foreseen in T4.2. Direct optical measurements for the $\boldsymbol{\alpha}$-Si case will be performed only if the validation activity in T4.2 will show discrepancies between simulation predictions and process characterizations. In the three tables below, we report the calibration assessment derived from the literature for the Si-related parameters in the three phases, respectively. Reference literature papers are indicated. We notice that some of these papers refer to a list of previous works where direct measurements are discussed.

Si crystal material calibration parameters			
Sym. [units]	Description	Expression	Ref.
$\rho\ [kg/m^3]$	Density	2320	(1)
$T_M\ [K]$	Melting Temp.	1688	(2)
$C\ [J/kg\ K\ ]$	T. Capacitance	$10\times T^{-1.034}/(1.02+0.01\times T) - 213$	(2)
$k\ [W\ /mK]$	T. Conductivity	$100\times((1523.7\times T^{-1.226})\times(T<1200)+(1523.7\times T^{-0.502})\times(T\geq 1200)$	(1)
$L\ [J/m^3]$	Latent Heat	1797000	(1)
$\varepsilon_r\ (308nm)[1]$	Permittivity Real	11.87	(1)
$\varepsilon_i(308nm)[1]$	Permittivity Im.	37.96	(1)
$A[m/s]$	Speed Pre-factor	1000	(1)
$E_a[eV]$	Activ. Energy	Range in 0.42-0.45	(1) (3)
$N\ [at/m^3]$	Atomic Density	4.995×10^{28}	(1)

Tab. 2: Crystal Si Material Parameters

Si liquid material calibration parameters			
Sym. [units]	Description	Expression	Ref.
$\rho\ [kg/m^3]$	Density	2520	(1)
$C\ [J/kg\ K\ ]$	T. Capacitance	1045	(2)
$k\ [W\ /mK]$	T. Conductivity	100 × [0.0502+0.000293× (T-T_M)]	(1)
$\varepsilon_r\ (308nm)[1]$	Permittivity Real	-15.734	(1)
$\varepsilon_i(308nm)[1]$	Permittivity Im.	10.126	(1)

Tab. 3: Liquid Si Material Parameters

Si (amorphous) material calibration parameters			
Sym. [units]	Description	Expression	Ref.
$\rho\ [kg/m^3]$	Density	2100	(2)
$T_M\ [K]$	Melting Temp.	1420	(1)
$C\ [J/kg\ K\ ]$	T. Capacitance	$10\times T^{-1.034}/(1.02+0.01\times T) - 213$	(2)
$k\ [W\ /mK]$	T. Conductivity	1.8	(1)
$L\ [J/m^3]$	Latent Heat	1317000	(1)
$\varepsilon_r\ (308nm)[1]$	Permittivity Real	0.333	(1)
$\varepsilon_i(308nm)[1]$	Permittivity Im.	21.11	(1)
$A[m/s]$	Speed Pre-factor	1000	(1)
$E_a[eV]$	Activ. Energy	0.32	(1)
$N\ [at/m^3]$	Atomic Density	Range in $4.9\text{-}4.995\times10^{28}$	(4) (1)

Tab. 4: Amorphous Si Material Parameters

We note that a heating problem which considers also melting phenomena requires the parameters appearing in the Fourier law (density, thermal capacitance and conductivity, latent heat) as well as a law of the temperature dependence for the solid-liquid interface speed v*(T)*. A Fulcher-Vogel law (5; 6) is usually assumed, which reads

$$v(T) = A\exp\left(-\frac{E_a}{k_bT}\right)\times\exp\left\{1-exp\left[\left(\frac{\rho L}{k_bN}\right)\left(\frac{1}{T_M}-\frac{1}{T}\right)\right]\right\}$$

where the symbols are defined in the table and k_b is the Boltzmann constant.

Germanium

Likewise silicon, the model calibration for germanium is reliable for the solid and the liquid phase (see table 1), while it has a less stable parameter setting for the amorphous phase. As a consequence, for the investigation of Ge-based structures we will follow the same strategy as for the Si-based ones: No request of direct optical measurements, but the eventual request of additional measurements only in the case of a partial failure of the code validation activity in task 4.2.

Ge crystal material calibration parameters			
Sym. [units]	Description	Expression	Ref.
$\rho\ [kg/m^3]$	Density	5320	(5)
$T_M\ [K]$	Melting Temp.	1210	(5)
$C\ [J/kg\ K\ ]$	T. Capacitance	1000 × (0.000117 × T + 0.293)	(5)
$k\ [W\ /mK]$	T. Conductivity	60.2 × (T / 300) $^{-1.25}$	(5)
$L\ [J/m^3]$	Latent Heat	465000	(5)
$\varepsilon_r\ (308nm)[1]$	Permittivity Real	$3.192\times10^{-6}\times T^2-1.355\times T+8.841$	(3)
$\varepsilon_i(308nm)[1]$	Permittivity Im.	$-5.2235\times10^{-6}\times T^2+1.593\times T+23.571$	(3)
$A\ [m/s]$	Speed Pre-factor	0.3×10^4	(5)
$E_a\ [eV]$	Activ. Energy	0.5	(5)
$N\ [at/m^3]$	Atomic Density	4.56×10^{28}	(5)

Tab. 5: Crystal Ge Material Parameters

Ge liquid material calibration parameters			
Sym. [units]	Description	Expression	Ref.
$\rho\ [kg/m^3]$	Density	1000 × (5.6 -0.000625 × (T - 1210))	(6)
$C\ [J/kg\ K\ ]$	T. Capacitance	460	(5)
$k\ [W\ /mK]$	T. Conductivity	29.7	(5)
$\varepsilon_r\ (308nm)[1]$	Permittivity Real	-16.225	(5)
$\varepsilon_i(308nm)[1]$	Permittivity Im.	9.993	(5)

Tab. 6: Liquid Ge Material Parameters

Ge amorphous material calibration parameters			
Sym. [units]	Description	Expression	Ref.
$\rho\ [kg/m^3]$	Density	5320	(5)
$T_M\ [K]$	Melting Temp.	987	(5)
$C\ [J/kg\ K\ ]$	T. Capacitance	1000 × (0.000172 × T + 0.2899)	(5)
$k\ [W\ /mK]$	T. Conductivity	2.5	(5)
$L\ [J/m^3]$	Latent Heat	350000	(5)
$\varepsilon_r\ (308nm)[1]$	Permittivity Real	-2.811	(5)
$\varepsilon_i(308nm)[1]$	Permittivity Im.	15.606	(5)
$A[m/s]$	Speed Pre-factor	0.3×10^4	(5)
$E_a[eV]$	Activ. Energy	0.5	(5)
$N\ [at/m^3]$	Atomic Density	4.12×10^{28}	(5)

Tab. 7: Amorphous Ge Material Parameters

SiGe alloy

SiGe is an almost ideal binary alloy system: Si and Ge are fully miscible in the whole range of composition. This fact generally makes the linear interpolation between the physical properties of Si and Ge (using the alloy fraction variable X) a good starting point for the calibration of this material (7). However, some critical uncertainties exist. A more accurate determination of the dependence of the optical parameters on X in each phase is necessary. Moreover, the dependence of the parameters in the disordered phases (liquid and amorphous) on X is barely determined by direct measurements: The usual approach here is the use of the same relations as for the crystal phase. In the tables we express all the parameters as

$$P_{SiGe}(T,X) = P_{Ge}(T)\times f^n_P(X) + P_{Si}(T) \times [1 - f^n_P(X)]$$

where $f^n_P(X)$ is monotonically growing polynomial function of degree n satisfying the obvious relationships $f_P(0) = 0$, $f_P(1)=1$ while $P_{Ge}(T)$ and $P_{Si}(T)$ are the Ge and Si parameters reported in the tables 1-6. Therefore, only $f^n_P(X)$ will be reported (see tables 8 – 10). In the case of linear interpolation we have:

$$f^n_P(X) = f^1_P(X) = X$$

We notice that the quadratic dependence of the solidus and liquidus curves, as described in Ref. (7), is effectively obtained in the phase field model by means of the combination of the linear dependence of the melting temperature T_M on X (see line 4 of table 8) and the segregation effect for X at the liquid-solid interface (1). An alternative calibration for the optical parameters is reported in Ref. (3) for the interval X≤0.4. This calibration will be also evaluated in the experimental tests.

SiGe crystal material calibration parameters			
Sym. [units]	Description	$f^n_P(X)$ (explanation see text)	Ref.
$\rho\ [kg/m^3]$	Density	1.2143×X- 0.2143 X^2	(7)
$T_M\ [K]$	Melting Temp.	X	(7)
$C\ [J/kg\ K\ ]$	T. Capacitance	X	(7)
$k\ [W\ /mK]$	T. Conductivity	X	(7)
$L\ [J/m^3]$	Latent Heat	X	(7)
$\varepsilon_r\ (308nm)[1]$	Permittivity Real	1.023×X – 0.023 X^2	(7)
$\varepsilon_i(308nm)[1]$	Permittivity Im.	1.469×X – 0.469 X^2	(7)
$A\ [m/s]$	Speed Pre-factor	X	(3)
$E_a\ [eV]$	Activ. Energy	X	(3)
$N\ [at/m^3]$	Atomic Density	X	(3)

Tab. 8: Amorphous Ge Material Parameters

SiGe liquid material calibration parameters			
Sym. [units]	Description	$f^n_P(X)$ (explanation see text)	Ref.
$\rho\ [kg/m^3]$	Density	1.2143×X- 0.2143 X^2	(7)
$C\ [J/kg\ K\ ]$	T. Capacitance	X	(7)
$k\ [W\ /mK]$	T. Conductivity	X	(7)
$L\ [J/m^3]$	Latent Heat	X	(7)
$\varepsilon_r\ (308nm)[1]$	Permittivity Real	1.023×X – 0.023 × X^2	(7)
$\varepsilon_i(308nm)[1]$	Permittivity Im.	1.469×X – 0.469 × X^2	(7)

Tab. 9: Liquid Ge Material Parameters

SiGe amorphous material calibration parameters			
Sym. [units]	Description	$f^{n}_{P}(X)$ (explanation see text)	Ref.
$\rho\ [kg/m^3]$	Density	1.2143×X- 0.2143 X^2	(7)
$T_M\ [K]$	Melting Temp.	X	(7)
$C\ [J/kg\ K\ ]$	T. Capacitance	X	(7)
$k\ [W\ /mK]$	T. Conductivity	X	(7)
$L\ [J/m^3]$	Latent Heat	X	(7)
$\varepsilon_r\ (308nm)[1]$	Permittivity Real	1.023×X - 0.023 X^2	(5)
$\varepsilon_i(308nm)[1]$	Permittivity Im.	1.469×X - 0.469 X^2	(7)
$A\ [m/s]$	Speed Pre-factor	X	(5)
$E_a\ [eV]$	Activ. Energy	X	(5)
$N\ [at/m^3]$	Atomic Density	X	(5)

Tab. 10: Amorphous Ge Material Parameters

SiO_2

First order phase transitions (i.e. latent heat absorption/release) do not occur for the SiO_2 material. T_M here is reported as the glass transition temperature since it could be of interest when the simulated temperature map is analyzed. The dependence of the thermal parameters on T is reliable. No direct optical measurements are necessary and constant values here reported are sufficient approximations for the early calibration set.

SiO_2 amorphous material calibration parameters			
Sym. [units]	Description	Expression	Ref.
$\rho\ [kg/m^3]$	Density	2203	(1)
$T_M\ [K]$	Glass transition temperature	1986	(1)
$C\ [J/kg\ K\ ]$	T. Capacitance	$1000 \times (0.604 + 5.188\times10^{-4} \times T)$	(1)
$k\ [W\ /mK]$	T. Conductivity	$100\times((1.005\times10^{-2}+1.005\times10^{-5}\times T)\times(T<1170)$ $+(2.512\times10^{-2}) \times (T\geq1170))$	(1)
$\varepsilon_r\ (308nm)[1]$	Permittivity Real	2.245	(1)
$\varepsilon_i(308nm)[1]$	Permittivity Im.	0.00036	(1)

Tab. 11: SiO_2 Material Parameters

HfO_2

First order phase transitions (i.e. latent heat absorption/release) do not occur for the HfO_2 material. T_M here is reported as the glass transition temperature, since it could be of interest when the simulated temperature map is analyzed. We use the thermal parameters reported for thin films. Actually, the same thermal diffusivity is reported for thick layers although the reported values of $k = 1\ [W\ /mK]$ and $C = 120\ [J/g\ K\ ]$ are different. Therefore, the simulation results obtained with the two choices of values are essentially equivalent. No direct optical measurements are necessary and constant values here reported are sufficient approximations for the early calibration set.

HfO_2 amorphous material calibration parameters			
Sym. [units]	Description	Expression	Ref.
$\rho\ [kg/m^3]$	Density	9680	(8)
$T_M\ [K]$	Glass transition temperature.	3031	(8)
$C\ [J/kg\ K\ ]$	T. Capacitance	60	(8)
$k\ [W\ /mK]$	T. Conductivity	0.5	(8)
$\varepsilon_r\ (308nm)[1]$	Permittivity Real	4.84	(9)
$\varepsilon_i(308nm)[1]$	Permittivity Im.	2.2×10^{-8}	(9)

Tab. 12: HfO_2 Material Parameters

Si_3N_4

First order phase transitions (i.e. latent heat absorption/release) do not occur for the Si_3N_4 material. T_M here is reported as the glass transition temperature since it could be of interest when the simulated temperature map is analyzed. The dependence of the thermal parameters on T is reliable. No direct optical measurements are necessary and constant values here reported are sufficient approximations for the early calibration set.

Si_3N_4 amorphous material calibration parameters			
Sym. [units]	Description	Expression	Ref.
$\rho\ [kg/m^3]$	Density	3100	(10)
$T_M\ [K]$	Glass transition temperature	2173	(10)
$C\ [J/kg\ K\ ]$	T. Capacitance	710	(10)
$k\ [W\ /mK]$	T. Conductivity	$(34\text{-}1.3310^{-2}\times T) \times (T\leq 1500)+14.05\times (T>1500)$	(10)

$\varepsilon_r\ (308nm)[1]$	Permittivity Real	5.087	(11)
$\varepsilon_i(308nm)[1]$	Permittivity Im.	0.2256	(11)

Tab. 12: Si_3N_4 Material Parameters

SiN

First order phase transitions (i.e. latent heat absorption/release) do not occur for the Si_3N_4 material. T_M here is reported as the glass transition temperature since it could be of interest when the simulated temperature map is analyzed. For a non-usual stoichiometry with respect to the 3/4 value we assume the same values of parameters as for the ideal case. No direct optical measurements are necessary and constant values here reported are sufficient approximations for the early calibration set.

SiN amorphous material calibration parameters			
Sym. [units]	Description	Expression	Ref.
$\rho\ [kg/m^3]$	Density	3100	(10)
$T_M\ [K]$	Glass transition temperature	2173	(10)
$C\ [J/kg\ K\ ]$	T. Capacitance	710	(10)
$k\ [W\ /mK]$	T. Conductivity	$2 + [\ 2.5\times10^{-5} \times (\ T - 420\ )^{2}\ ] \times (\ T \geq\ 420)$	(10)
$\varepsilon_r\ (308nm)[1]$	Permittivity Real	5.087	(11)
$\varepsilon_i(308nm)[1]$	Permittivity Im.	0.2256	(11)

Tab. 13: SiN Material Parameters

TiN

Due to the high melting point, melting is not activated in the TiN material regions. Therefore, melting related parameters are not considered in the modelling. The melting temperature is reported since it could be of interest when the simulated temperature map is analyzed. The dependence of the thermal parameters on T is reliable. No direct optical measurements are necessary and constant values here reported are sufficient approximation for the early calibration set.

TiN solid material calibration parameters			
Sym. [units]	Description	Expression	Ref.
$\rho\ [kg/m^3]$	Density	5400	(12)
$T_M\ [K]$	Melting Temp.	3203	(12)

$C\ [J/kg\ K\ ]$	T. Capacitance	590.9082 × (T < 293) + 913.71045 × (T > 1800) + [3.8938×10 $^{-13}$×T^5 - 2.3260×10^{-9}×T^4 + 5.4317×10^{-6}×T^3 - 0.00622795×T^2 + 3.623921786×T - 43.86595639] × (T ≥293) × (T ≤ 1800)	(12)
$k\ [W\ /mK]$	T. Conductivity	27.438 × (T < 298.15) + 9.023 × (T > 1273.15) + [2.83579 × 10^{-5} × T^2 - 0.063446492 × T + 43.83391717] × (T ≥ 298.15) * (T ≤ 1273.15)	(12)
$\varepsilon_r\ (308nm)[1]$	Permittivity Real	4.2714	(13)
$\varepsilon_i(308nm)[1]$	Permittivity Im.	5.4902	(13)

Tab. 14: TiN Material Parameters

W

Due to the high melting point, melting is not activated in the W material regions. Therefore, melting related parameters are not considered in the modelling. The melting temperature is reported since it could be of interest when the simulated temperature map is analyzed. The dependence of the thermal parameters on T is reliable. No direct optical measurements are necessary and constant values here reported are sufficient approximation for the early calibration set.

W solid material calibration parameters			
Sym. [units]	Description	Expression	Ref.
$\rho\ [kg/m^3]$	Density	-4.4717×10^{-5} × T^2 - 1.7140 × 10^{-1} × T + 19404.83	(14)
$T_M\ [K]$	Melting Temp.	3683	(14)
$C\ [J/kg\ K\ ]$	T. Capacitance	-3.9836×10^{-15}×T^5+4.5292×10^{-11}×T^4– 1.9763×10^7×T^3 + 4.1504×T^2 - 4.3211×10^{-1}× T + 271.1924	(14)
$k\ [W\ /mK]$	T. Conductivity	27.438 × (T < 298.15) + 9.023 × (T > 1273.15) + [2.83579 × 10^{-5} × T^2 - 0.063446492 × T + 43.83391717] × (T ≥ 298.15) * (T ≤ 1273.15)	(14)
$\varepsilon_r\ (308nm)[1]$	Permittivity Real	-15.413	(15)
$\varepsilon_i(308nm)[1]$	Permittivity Im.	14.818	(15)

Tab. 15: W Material Parameters

Pt

The Pt melting point is relatively high with respect to the ones of the semiconductor materials; as a consequence the eventual melting is neglected and it is only considered as a warning in the simulation (i.e. an extreme of the process window). Similarly to W and TiN, melting related parameters are not considered in the modelling. The melting temperature is reported since it could be of interest when the simulated temperature map is analyzed. The dependence of the thermal parameters on T is reliable. No direct optical measurements are necessary and constant values here reported are sufficient approximations for the early calibration set.

Pt solid material calibration parameters			
Sym. [units]	Description	Expression	Ref.
$\rho\ [kg/m^3]$	Density	21450	(16)
$T_M\ [K]$	Melting Temp.	2046	(16)
$C\ [J/kg\ K\ ]$	T. Capacitance	125.604	(17)
$k\ [W\ /mK]$	T. Conductivity	$64 + 1.7 \times 10^{-2} \times T$	(16)
$\varepsilon_r\ (308nm)[1]$	Permittivity Real	-6.5769	(15)
$\varepsilon_i(308nm)[1]$	Permittivity Im.	6.4943	(15)

Tab. 15: Pt Material Parameters

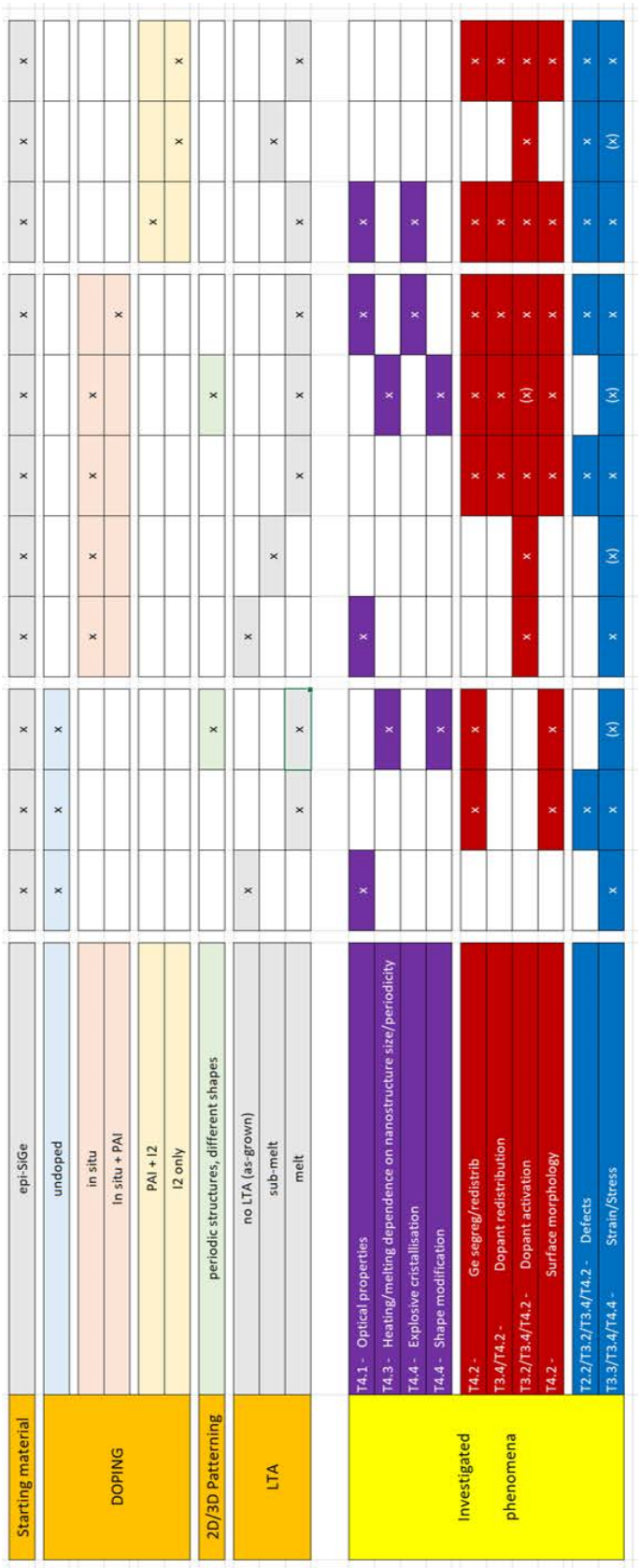

Fig. 1 Design of Experiments (DOE) summary table. In the orange section the crosses indicate the combination of processes for the sample preparations (e.g. column 2 of the matrix indicates undoped SiGe undergoing a melting laser process).

4. Optical measurements plan

The calibration scenario discussed in the previous section clearly shows that an experimental campaign for the direct measurements of optical parameters should mainly focus on the SiGe material also due to the additional dependence of the permittivity on the alloy fraction value. Additional measurements on different materials will be performed only if: a) there will be some critical issues of the calibration validation by means of comparison between simulations and measurements on post-irradiated samples, b) an urgent technological interest during the MUNDFAB project development.

In Fig. 1, a matrix showing the Design of Experiments (DOE) summary is reported. As we can notice, the same set of samples can impact on different investigation themes in WP4 and other WPs. The complex permittivity will be measured in a temperature range (from RT to 600°C) which is the maximum possible extension for the ellipsometry measurements. In the determination of this range we consider the equipment available within the MUNDFAB consortium.

We notice that each point of the DOE scheme corresponds also to different values of material parameters. In the following we clarify these DoE additional variables which are not visible in the compact 2D map of Fig.1. Undoped samples will be fabricated with different values of the alloy fraction (10%, 20%, 30% 40% Ge). Amorphous SiGe (together with l-SiGe) is indicated as the most critical case for the calibration since it combines the complexity of the amorphous phase and ones of the alloy. Amorphous samples will be available for the same cited cases as crystalline ones, including pure Si and Ge. Indeed, a necessity of measurements for the pure elemental phase could emerge during the project (see also table 1 and comments in the previous section). These samples will be amorphized by implantation after the epitaxial growth (Pre-Amorphization Implantation i.e PAI in Fig.1). It is worth noting that the measurements in the whole temperature range (RT-600°C) could be challenging due to the metastability of the amorphous phase. The reliable temperature range for the optical measurements in the case of amorphous materials will be specifically determined.

Doped SiGe samples at fixed alloy fraction of 30% Ge will be fabricated with three different levels of in-situ B doping in the range between 5×10^{19} - 5×10^{20} cm^{-3}. The actual B density will be determined by means of accurate SIMS measurements before further processing and/or analyses. Also these sample will be amorphized to verify the possible role of dopant atoms in the **α**-SiGe optical properties.

In parallel to the in-situ doped samples, implantation will be also used to add impurities in both the crystalline and the amorphous samples. Focused samples will be also measured after the implantation in order to verify that permittivity is not modified with respect to the pristine evaluation.

An important observation is that all measurements will be performed in 30 nm thick SiGe layers epitaxially grown on a Si substrate. This should be a good setting for the measurements also considering the strong absorption of the 308nm laser light. However, relaxed 200nm thick SiGe layers will be also grown for the fabrication of patterned structures (see next section); therefore, if necessary, these samples will be also available for the optical measurements.

5. Laser irradiation experimental plan

Samples after the different preparation conditions discussed in the previous chapter will be irradiated with the pulsed excimer laser annealing system available at CEA-LETI (308 nm wavelength, 160 ns pulse duration) on 15 × 15 mm^2 areas, considering a wide energy density range. In the case of blanket SiGe samples (from 0% to 100% of the Ge alloy fraction), we have verified, by means of simulations performed with the current calibration setting, that a fluence range from 1. to 2.5 J/cm^2 is suitable to cover a wide range of regimes and melting depths. This range includes sub-melt; the full melt of the epitaxially grown layer; and, finally, to extend the melting to the underlying substrate. Single-pulse mode and multiple pulses mode will be considered (2,5,10 pulses). Replicas of the process cases will be considered to split the samples for the different characterization analyses planned in the planar case (see the brief outline in the following). Focused samples will be also analyzed with ellipsometry after irradiation. By means of these analyses supported by process simulations and chemical profile measurements, we will also attempt to extend the calibration to regimes that are not considered in the pre-LA cases discussed in section 2.

In addition to the blanked samples, 2D and 3D patterned samples will be fabricated with the aid of top-down nano-patterning (electron beam lithography and plasma etching) in two classes of samples (undoped and in-situ doped, see Fig. 1, with thicknesses of 30 nm and 200nm of the SiGe layer). Critical dimensions of 2D structures (Fins) will be in the range of 20 nm to 60 nm in width whilst critical dimensions of 3D structures (nanowires) will be in range of 15 nm to 60 nm in diameter. The pitch (periodicity) will be in the 100-300nm range. Patterning materials will be SiOx oxides. In the case of patterned samples, early evaluation with simulations indicated that we should downshift the interesting range of fluences by about 0.5 J/cm^2.

As indicated in the technical annex, the following characterization plan will be followed:

- Atomic species redistribution (both impurity density and alloy fraction) will be extracted by SIMS.
- Conventional TEM analyses and investigations of the crystalline quality by High Resolution TEM (HRTEM).
- Measurements of the modification of the SiGe stoichiometry and of highly doped 2D chemical profiles by the STEM-EDX technique.
- Measurements of 1D active dopant profiles with nanometer resolution by Differential Hall effect.
- Measurements of 2D active profiles using the SCM and SSRM techniques.
- AFM and SEM topographies.
- HR-XRD analyses of strain.

6. Conclusions

In this deliverable we have provided the early calibration details for the materials of interest for the WP4 derived by means of a literature analysis. We will use this calibration “ex ante” for any pre-evaluation of LA processes in the MUNDFAB project. Therefore, the current calibration will be implemented in a customized code available at the CNR and at the CEA. An important goal of further investigation for the WP4 will be the refinement and the definitive assessment of this

calibration. The planning for the direct (optical) measurements and experiments aiming at the model validation, but also at the indirect determination of parameters by fitting procedures, has been also presented.

References

1. *A phase-field approach to the simulation of the excimer laser annealing process in Si.* **A. La Magna, P. Alippi, V. Privitera, G. Fortunato, M. Camalleri, B. Svensson.** 9, s.l. : AIP, 2004, JOURNAL OF APPLIED PHYSICS, Vol. 95, p. 4806.

2. **A S. Okhotin, A. S. Pushkarskii, and V. V. Gorbachev.** *Thermophysical Properties of Semiconductors.* Moskov : "Atom" Publ. House,, 1972.

3. *Pulsed laser annealing for advanced technology nodes: Modeling and calibration.* **K. Huet, J. Aubin, P.-E. Raynal, B. Curvers, A. Verstraete, B. Lespinasse, F. Mazzamuto, A. Sciuto, S.F. Lombardo, A. La Magna, P. Acosta-Albad, L. Dagaultd. C. Licitra, J.-M. Hartmann, S. Kerdilès.** 0169-4332, Amsterdam : Volume 505, 1 March 2020, 144470, 2020, Vol. 505, p. 144470.

4. *Density of amorphous Si.* **Thompson, J. S. Custer and M. O.** 1994, Appl. Phys. Lett., Vol. 64, p. 437.

5. *Phase field model of the nanoscale evolution during the explosive crystallization phenomenon.* **S. F. Lombardo, S. Boninelli, F. Cristiano, I. Deretzis, M. G. Grimaldi, K. Huet, E. Napolitani and A. La Magna.** s.l. : AIP, 2018, JOURNAL OF APPLIED PHYSICS, Vol. 123, p. 105105.

6. *Interfacial transport kinetics during the solidification of silicon.* **S. Stiffler, P. Evans, and A. Greer.** s.l. : Elsevier, 1992, Acta Metallurgica et Materialia, Vol. 1617, p. 40.

7. **F., Schaffler.** *in "Properties of Advanced SemiconductorMaterials GaN, AlN, InN, BN, SiC, SiGe".* New York : Eds. Levinshtein M.E., Rumyantsev S.L., Shur M.S., John Wiley & Sons, Inc., 2001. pp. 149-188.

8. *Thermal Properties of Ultrathin Hafnium Oxide Gate Dielectric Films.* **M. A. Panzer, M. Shandalov, J. A. Rowlette, Y. Oshima, Y. W. Chen, P. C. McIntyre, and K. E. Goodson.** 12, 2009 , IEEE ELECTRON DEVICE LETTERS, Vol. 30, p. 1269.

9. *A study of some optical properties of hafnium dioxide (HfO2) thin films and their applications.* **M. Fadel, O.A. Azim, O.A. Omer, R.R. Basily.** 1998 , Appl. Phys. A , Vol. 66 , p. 335.

10. *THE EFFECT OF CRUCIBLE COATING AND THE TEMPERATURE FIELD ON MINORITY CARRIER LIFETIME IN DIRECTIONALLY SOLIDIFIED MULTICRYSTALLINE SILICON INGOTS.* **B. Ryningen, M. P. Bellmann1, R. Kvande, O. Lohne.** 2012, 27th European Photovoltaic Solar Energy Conference and Exhibition, p. 926.

11. *Optical Properties, Band Gap, and Surface Roughness of Si3N4.* **Bauer, J.** 1977, phys. stat. sol. (a) , Vol. 39, p. 411.

12. *Thermal conductivity of nitride films of Ti, Cr, and W deposited by reactive magnetron sputtering.* **Jagannadhama, K.** 2015, Journal of Vacuum Science & Technology A , Vol. 33, p. 031514 .

13. *Optical Properties and Plasmonic Performance of Titanium Nitride.* **P. Patsalas, N. Kalfagiannis and S. Kassavetis.** 6, 201, Materials , Vol. 8, p. 3128 .

14. **Shabalin, Igor L.** *Ultra-High Temperature Materials.* s.l. : Springer, 2014. p. 237. Vol. 4. 978-94-007-7586-2.

15. *Optical Constants and Inelastic Electron-Scattering Data for 17 Elemental Metals.* **W. S. M. Werner, K. Glantschnig, C. Ambrosch-Draxl.** 4, s.l. : American Institute of Physics, 2009, J. Phys. Chem. Ref. Data, Vol. 38, p. 1013.

16. *Platinum as a Thermal Conductivity Standard.* **Slack, G.A.** 2, s.l. : AIP, 1964, Jour. of Appl. Phys. , Vol. 35, p. 339.

17. *3-omega method for specific heat and thermal conductivity measurements.* **L. Lu, W. Yi, and D. L. Zhang.** 7, s.l. : AIP, 2001, REVIEW OF SCIENTIFIC INSTRUMENTS , Vol. 72.